Biochimica et Biophysica Acta 1812 (2011) 1435–1445

Contents lists available at ScienceDirect

Biochimica et Biophysica Acta

journal homepage: www.elsevier.com/locate/bbadis

Natural phenylalanine hydroxylase variants that confer a mild phenotype affect the enzyme's conformational stability and oligomerization equilibrium

Monica Cerreto [a,1], Paola Cavaliere [a,b,1], Carla Carluccio [a,c], Felice Amato [a], Adriana Zagari [a,b], Aurora Daniele [a,d,e,*], Francesco Salvatore [a,c,e,**]

[a] CEINGE–Biotecnologie Avanzate Scarl, Naples, Italy
[b] Dipartimento di Scienze Biologiche, Università di Napoli "Federico II", Naples, Italy
[c] Dipartimento di Biochimica e Biotecnologie Mediche, Università di Napoli "Federico II", Naples, Italy
[d] Dipartimento di Scienze Ambientali, Seconda Università di Napoli, Caserta, Italy
[e] IRCCS – Fondazione SDN, Naples, Italy

ARTICLE INFO

Article history:
Received 8 March 2011
Received in revised form 19 July 2011
Accepted 20 July 2011
Available online 27 July 2011

Keywords:
BH4 responsiveness
Number and brightness
PAH conformational stability
PAH oligomerization equilibrium
Hyperphenylalaninemia
Phenylalanine hydroxylase

ABSTRACT

Hyperphenylalaninemias are genetic diseases prevalently caused by mutations in the phenylalanine hydroxylase (*PAH*) gene. The wild-type PAH enzyme is a homotetramer regulated by its substrate, cofactor and phosphorylation. We reproduced a full-length wild-type protein and seven natural full-length PAH variants, p.I65M, p.N223Y, p.R297L, p.F382L, p.K398N, p.A403V, and p.Q419R, and analyzed their biochemical and biophysical behavior. All mutants exhibited reduced enzymatic activity, namely from 38% to 69% of wild-type activity. Biophysical characterization was performed by size-exclusion chromatography, light scattering and circular dichroism. In the purified wild-type PAH, we identified the monomer in equilibrium with the dimer and tetramer. In most mutants, the equilibrium shifted toward the dimer and most tended to form aggregates. All PAH variants displayed different biophysical behaviors due to loss of secondary structure and thermal destabilization. Specifically, p.F382L was highly unstable at physiological temperature. Moreover, using confocal microscopy with the number and brightness technique, we studied the effect of BH4 addition directly in living human cells expressing wild-type PAH or p.A403V, a mild mutant associated with BH4 responsiveness in vivo. Our results demonstrate that BH4 addition promotes re-establishment of the oligomerization equilibrium, thus indicating that the dimer-to-tetramer shift in pA403V plays a key role in BH4 responsiveness. In conclusion, we show that the oligomerization process and conformational stability are altered by mutations that could affect the physiological behavior of the enzyme. This endorses the hypothesis that oligomerization and folding defects of PAH variants are the most common causes of HPAs, particularly as regards mild human phenotypes.

1. Introduction

Phenylketonuria (PKU, Online Mendelian Inheritance in Man database: 261600) and its hyperphenylalaninemia (HPA) variants represent the most common inherited disorder of amino acid metabolism transmitted by an autosomal recessive mode [1]. The primary cause of HPA is a dysfunction of phenylalanine hydroxylase (PAH: EC 1.14.16.1). In the liver, this enzyme metabolizes L-Phenylalanine (L-Phe) to L-Tyrosine (L-Tyr) using (6R)-L-erythro-5,6,7,8-tetrahydrobiopterin (BH4) as coenzyme. More rarely, forms of HPAs can also be caused by a lack of the BH4 cofactor due to defective cofactor biosynthesis and regeneration [2]. Untreated PKU patients present an abnormal phenotype, with growth failure, microcephaly, seizures and permanent neurologic damage because their body fluids contain elevated levels of L-Phe and its neurotoxic metabolites (phenylpyruvate, phenylacetate and phenylactate) [1,3].

The major manifestations of the disease, which start at birth, are prevented by severe dietary restriction of L-Phe [4] and, in selected cases, by BH4 supplementation, which reduces L-Phe levels and increases L-Phe tolerance in HPA patients [5]. Several new therapeutic strategies based on the biochemistry and pathogenetic features of PKU are currently being investigated [6,7].

Abbreviations: BH4, (6R)-L-erythro-5,6,7,8-tetrahydrobiopterin; CD, circular dichroism; Δ13-PAH, PAH missing residues 1–13; DSC, differential scanning calorimetry; Ek, enterokinase; HPA, hyperphenylalaninemia; IPTG, isopropylthio-β-D-galactoside; L-Phe, phenylalanine; LS, light scattering; MALS, multiangle light scattering; MBP, maltose-binding protein; N&B, number and brightness; PKU, phenylketonuria; SEC, size-exclusion chromatography

* Correspondence to: A. Daniele, CEINGE–Biotecnologie Avanzate Scarl, Via Gaetano Salvatore 486, 80145 Naples, Italy.
** Correspondence to: F. Salvatore, CEINGE–Biotecnologie Avanzate Scarl and Dipartimento di Biochimica e Biotecnologie Mediche, Università di Napoli "Federico II", Via Sergio Pansini 5, Ed.19, 80131 Naples, Italy. Tel.: +39 0817463133; fax: +39 0817463650.
E-mail address: salvator@unina.it (F. Salvatore).
[1] These authors contributed equally to this paper.

0925-4439/$ – see front matter © 2011 Elsevier B.V. All rights reserved.
doi:10.1016/j.bbadis.2011.07.012

The human *PAH* gene, mapped on 12q23.2, consists of 13 exons encompassing 171 kb. The full-length *PAH* cDNA encodes a protein of about 52 kDa (452 amino acids) that in the mature form is assembled as a homotetramer. Each subunit consists of three functional domains: a flexible N-terminal regulatory domain (residues 1–142); a catalytic domain (residues 143–410) that includes binding sites for iron, substrate and cofactor; and a C-terminal oligomerization domain (residues 411–452) with dimerization (residues 411–426) and tetramerization motifs (residues 427–452) [8] (Fig. 1). The crystal structure of PAH has revealed that the tetrameric oligomers are dimers of dimers in which the interaction between the two dimers is mediated by the C-terminal 'arm' [8].

The tetrameric and dimeric forms of PAH are in equilibrium [9,10] and have different catalytic properties because the tetramer, but not the dimer, demonstrates a positive kinetic cooperativity with respect to L-Phe [11]. In particular, substrate activation results in conformational changes involving the tertiary as well as the quaternary structure [12] and drives the tetramer–dimer equilibrium toward the tetrameric form [13]. Further regulation mechanisms require binding of BH4 [12] and phosphorylation [14].

The clinical and metabolic features associated to HPA are complex [15] and various genotype–phenotype correlation studies have been performed [16–18]. In addition, at molecular level, about 600 mutations have been identified, most of which are point mutations scattered throughout the whole *PAH* gene (http://www.pahdb.mcgill.ca), although frequencies differ among populations and geographic areas [16–18].

Recombinant variant proteins containing prevalently missense mutations have been analyzed and characterized in vitro; each mutation exerts a distinct effect on the behavior of the PAH protein, which in many cases allows the prediction of the biochemical phenotype [19–21]. The effects of a specific mutation on protein functions have been studied with different approaches, i.e., enzyme assay, in vivo isotopic studies and in vitro expression. Moreover, the crystal structures of human and rat PAH [8,22] provided the structural basis of HPA [23]. It is now established that, in most HPA cases, the loss of PAH function is due to decreased stability [21,24], increased susceptibility toward aggregation and degradation of PAH mutant proteins [19,24,25], thermodynamic instability [26] and/or folding efficiency [27]. About 75% of PAH mutations, characterized by high residual activity, have been found to be associated with BH4 responsiveness, both in vitro [28–30] and in vivo [4,5]. It has recently been speculated that pharmacological doses of BH4 may augment the conformational stability and the amount of functional PAH [31].

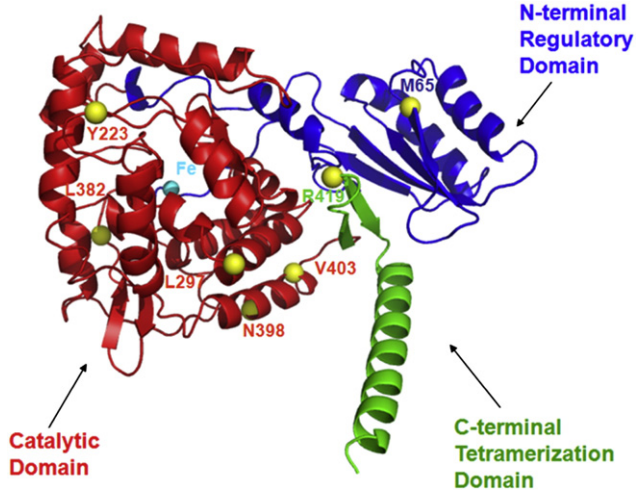

Fig. 1. Full-length composite model of the PAH monomer structure and distribution of the HPA-related missense mutations studied in this paper. The N-terminal regulatory domain is shown in blue, the catalytic domain in red and the tetramerization domain in green. The Fe ion is shown as a cyan sphere at the center of the catalytic domain; the mutation sites are marked as yellow balls.

We previously carried out a molecular analysis of the *PAH* gene in HPA patients from Southern Italy, and identified and characterized several novel mutations [32–34]. In the present study, we analyzed the wild-type PAH protein and some PAH natural mutants to obtain further information about the molecular basis of HPAs and the mechanism of BH4 responsiveness. To this purpose, we reproduced, by in vitro mutagenesis, the wild-type and seven natural variants of PAH: p.I65M, p.N223Y, p.R297L, p.F382L, p.K398N, p.A403V, and p.Q419R, and characterized the biophysical–biochemical properties of the above-mentioned purified full-length proteins in order to understand the impact of each mutation on the activity, oligomeric structure and stability of PAH. In addition, we investigated the mechanism underlying BH4 responsiveness using p.A403V, which is one of the most frequent mutations in our geographic area [32], and is associated with a BH4-responsive mild phenotype [35].

2. Material and methods

2.1. Construction of PAH expression plasmid and site-directed mutagenesis

PAH wild-type and mutant constructs were obtained by modifying the pMAL Xa PAH plasmid, kindly provided by Drs CR. Scriver and P. Waters (McGill University-Montreal Children's Hospital Research Institute, Montreal, Canada), to digest the fusion protein MBP-PAH with enterokinase (Ek) [9]. The Ek site was inserted downstream the sequence encoding the factor Xa site, by site-directed mutagenesis using the primers 5′gatgacgatgacaagtctactgcggtcctgg3′ and 5′ gccctaactcccttccctactgctactgttc3′ and the Quick Site-directed mutagenesis kit (Stratagene, CA, USA). GFP was amplified by PCR from pEGFP-N1 (Clonetech, CA, USA) using the primers: 5′acattaggtaccagccatggtgagcaagggcgag3′ and 3′ gtagatgaattctccaccacccttgtacagctcg 5′ and cloned into pcDNA3 (Invitrogen, Carlsbad, CA) using Kpn1 and EcoR1 sites. PAH cDNA was amplified from pMAL Xa Ek PAH by using the primers: 5′catcattgaattctccactgcggtcctgg3′ and 3′ cgtaatgcggccgcttactttattttctggag 5′ and cloned downstream GFP, using EcoR1 and Not1 sites. Sequence analysis confirmed the correct frame.

Mutations were introduced into pMAL Xa Ek PAH and pCDNA3-GFP-PAH using mutagenic primers and the Quick Site-directed mutagenesis kit (Table 1). The modified plasmid and the mutant clones were sequenced to verify the introduction of each single mutation. Commercial MBP was obtained from New England Biolabs (Ipswich, MA, USA).

2.2. Expression, purification and N-terminal sequencing of the PAH protein

pMAL Xa Ek PAH expression plasmids were transformed into *Escherichia coli* BL21 cells and the colonies were selected using Luria-Broth plates with ampicillin (0.1 mg mL^{-1}). Bacteria were grown to 2×10^8 cells/mL (A_{600nm}~0.5) and overexpression of wild-type and variant MBP-PAH fusion proteins was induced with 1 mM isopropylthio-β-D-galactoside (IPTG) for 16 h at 37 °C. Cells were harvested by centrifugation and treated according to the instruction manual of the pMAL protein fusion and purification system (New England Biolabs). The fusion protein was digested overnight at room temperature with Ek (New England Biolabs) to obtain wild-type and mutant forms of PAH without the MBP tag, using 0.5 ng of enzyme for each 50 μg fusion protein. The mixture was then applied to a hydroxyapatite column (1 cm × 10 cm, Bio-Rad Laboratories, CA, USA) and subjected to several washes with 20 mM sodium phosphate, 200 mM NaCl (pH 7.2). Proteins were then eluted with 0.5 M Na phosphate, pH 7.2 and subsequently MBP was isolated from the

Table 1
The seven mutant forms of PAH reproduced in vitro as recombinant products and analyzed. The primer pairs used to produce the pMAL Xa Ek PAH plasmid.

Mutant forms of PAH	Mutagenic primers (forward)	Mutagenic primers (reverse)
Ek site	5′GATGACGATGACAAGTCTACTGCGGTCCTGG3′	5′GCCCTAACTCCCTTCCCTACTGCTACTGTTC3′
p.I65M	5′ACCTGACCCACATGGAATCTAGACCTTCTC3′	5′GAGAAGGTCTAGATTCCATGTGGGTCAGGT3′
p.N223Y	5′CATGAAGATTACATTCCCCAGCTGGAAGAC3′	5′GTCTTCCAGCTGGGGAATGTAATCTTCATG3′
p.R297L	5′TGTTTTCAGATCTCAGCTTTGCCCAGTTTT3′	5′AAAACTGGGCAAAGCTGAGATCTGAAAACA3′
p.F382L	5′ACTGTCACGGAGTTGCAGCCCCTGTATTAC3′	5′GTAATACAGGGGCTGCAACTCCGTGACAGT3′
p.K398N	5′GCCAAGGAGAACGTAAGGAACTTTGCTGCC3′	5′GGCAGCAAAGTTCCTTACGTTCTCCTTGGC3′
p.A403V	5′GAAAGTAAGGAACTTTGTTGCCACAA3′	5′CCGAGGTATTGTGGCAACAAAGTTCC3′
p.Q419R	5′ATACACCCGAAGGATTGAGG3′	5′CCTCAATCCTTCGGGTGTAT3′

cleavage mixture by re-binding to amylose resin. PAH was finally purified by size-exclusion chromatography with a HiLoad 16/60 Superdex 200 column (GE Healthcare, UK). Protein concentrations were determined spectrophotometrically with the use of the absorption coefficient A280 or the dye-binding Bradford assay (Bio-Rad Laboratories). The N-terminal amino acid sequence of PAH was determined by Edman degradation on an automated Procise H49 sequencer (Applied Biosystems, MA, USA).

It has been reported [36] that, during the various steps of recombinant protein production, some labile Asn residues are deamidated: however, any possible deamidation of these residues, which would in the activity assay produce substrate inhibition, would most likely be the same in the presence of wild-type and of the variant forms of PAH we have employed.

2.3. Concentration and storage of proteins

The concentration of proteins was determined both by the micro BCA protein assay and spectrophotometrically. The final protein concentration was measured based on optical density at 280 nm using, for the extinction coefficient, a value of 49,780, 66,350 and 115,630 M^{-1} cm^{-1} for PAH, MBP and the fused wild-type MBP-PAH respectively, deduced from the amino acid composition of the protein. We used a SpeedVac concentrator (Thermo Scientific, Rockford, IL, USA) to concentrate the protein solutions because ultra-filtration led to considerable sample loss. All protein samples, if not utilized within few days, were stored at −20 °C in their elution buffer (see below).

2.4. PAH activity and thermal inactivation assay

Enzymatic activity analysis was carried out on a whole equilibrium mixture of oligomeric species of purified full-length wild-type and mutant PAH (see Supplementary Table S1). The activity was assayed in the presence of 0.25 μCi L-[^{14}C] Phe (Amersham, Buckinghamshire, UK; 460 μCi/mmol); 0.25 mM cold L-Phe, 1.3 units of beef liver catalase; 0.8 mM BH4; 250 mM Tris HCl pH 7.8, 1 μg of protein; final volume: 100 μL. The reaction was conducted at 25 °C with an incubation time of 1 h [32–34]. After centrifugation at room temperature and maximum speed, an aliquot of each supernatant was applied on a thin-layer chromatography system and the amount of [^{14}C] radio-labeled L-Phe converted to [^{14}C] radio-labeled L-Tyr was measured. The mean PAH activities were calculated from three sets of experiments. The residual activities of mutant PAH enzymes were expressed as a percentage of wild-type enzyme activity. The same assay was used for the thermal inactivation analysis of the wild-type protein and of the p.F382L mutant. Thermal inactivation of both proteins was determined by measuring the decay of tyrosine production as a function of temperature in the 32–58 °C range.

2.5. Electrophoresis and immunoblotting

SDS/PAGE was performed at 100 V (2 h) in a 10% (w/v) polyacrylamide gel. The purification of all proteins was verified after staining with Colloidal Coomassie. The absence of MBP contamination in all preparations was determined by western blot analyses. Immunoblotting was performed using affinity-purified rabbit anti-hPAH [32–34] and mouse anti-MBP (New England Biolabs) as primary antibodies. The enhanced chemiluminescence system from Amersham (GE Healthcare) was used for immunodetection.

2.6. Size-exclusion chromatography with multiangle light scattering

Size-exclusion chromatography (SEC) was performed using Akta FPLC chromatography equipment (GE Healthcare) on a Superdex 200 10/300 GL column. The column was previously calibrated for molecular mass using a Gel Filtration High Molecular Weight calibration kit (GE Healthcare) constituted by ovalbumin (44 kDa), conalbumin (75 kDa) and aldolase (158 kDa). Before each run, the column was equilibrated with at least two column volumes of elution buffer and each run was performed at both 4 °C and room temperature (20–23 °C). The elution buffer was Tris–HCl 20 mM pH 7.4, NaCl 100 mM (buffer A) and, in a few cases, Na-phosphate 20 mM pH 7.0, KF 150 mM (buffer B).

The eluent flow was 0.5 mL min^{-1}. Only freshly prepared or recently defrosted proteins were loaded on the column because storage at 4 °C for more than one week led to sample aging. A total of 0.1 ÷ 0.2 mg of proteins were loaded. At room temperature, the elution profile was monitored at three UV absorption wavelengths (280 nm, 215 nm and 258 nm). At 4 °C, UV absorption was measured only at 280 nm. The chromatograms were deconvoluted by Unicorn software, supplied with the FPLC device, to calculate the percentage of single species. All chromatograms were normalized in the (0.0 ÷ 1.2) range.

At room temperature, size-exclusion chromatography with multiangle light scattering (MALS) experiments was carried out with the AKTA system coupled to a three-angle (45°, 90° and 135°) Wyatt Minidown EOS light scattering instrument linked to a Wyatt Optilab refractometer (Wyatt Technology Corp., Santa Barbara, CA). These experiments served to determine the sizes of oligomers of wild-type and mutant PAH. Molecular masses, polydispersity and root mean square radius calculations were made by ASTRA software, which is supplied with the light scattering device, using a dn/dc value of 0.185 mL g^{-1}.

2.7. Circular dichroism

Circular dichroism (CD) analysis was performed on commercial MBP, on the fused wild-type MBP-PAH tetrameric sample and on the most abundant species of cleaved PAH proteins after SEC purification. In the case of the cleaved wild-type PAH, CD experiments were performed with both the tetrameric form and the whole equilibrium mixture. A 2-day dialysis at 4 °C against Tris–HCl 20 mM pH 7.4 (buffer C) was conducted to eliminate NaCl before CD experiments. All CD spectra were recorded with a Jasco J-810 spectropolarimeter equipped with a Peltier temperature control system (model PTC-423-S). The spectropolarimeter was calibrated with an aqueous solution of D-10-(+)-camphorsulfonic acid at 290 nm. The molar ellipticity per mean residue, $[\theta]$ in deg cm^2 $dmol^{-1}$, was calculated from the equation $[\theta] = [\theta]_{obs}$ mrw $(10\ l\ C)^{-1}$, where $[\theta]_{obs}$ is the ellipticity measured in degrees, mrw is the mean residue molecular weight (111.5 Da), C is the protein concentration in

g mL^{-1}, and l is the optical path length of the cell in cm. Far-UV (ultraviolet) measurements (190–260 nm) were carried out at 20 °C using a 0.2 cm optical path length cell and a protein concentration in the range 0.10–0.15 mg mL^{-1}. CD spectra, recorded with a time constant of 4 s, a 1-nm bandwidth, and a scan rate of 20 nm min^{-1}, were signal averaged over at least three scans. The baseline was corrected by subtracting the buffer spectrum. Thermal denaturation curves were recorded over the 20–80 °C temperature range and by monitoring the CD signal at 222 nm. After preliminary trials within the scan rate interval of 0.5 ÷ 2.0 °C min^{-1}, all curves were recorded using a 0.2-cm path length cell and a scan rate of 1.0 °C min^{-1}. Irreversibility of the denaturation was verified by recording, after cooling to 20 °C, the spectra of samples subjected to a first temperature scan. All denaturation curves were normalized in an interval of 0.0 ÷ 1.0. The T_m values were determined from the first derivatives of the denaturation curves after noise reduction by using the standard analysis program provided with the instrument.

2.8. Cell culture

HeLa cells were grown in D-MEM high glucose medium (Invitrogen) containing 10% heat inactivated fetal bovine serum (Invitrogen), 1% penicillin/streptomycin, at 37 °C in 5% CO_2. Transfections of both wild-type PAH and the p.A403V mutant were carried out using the ProFection Mammalian Transfection System (Promega, WI, USA) in accordance with the manufacturer's protocol. Cells were plated on 35-mm glass bottom dishes (MatTek, MA) for imaging.

2.9. Confocal microscopy and number and brightness analysis

Constructs containing GFP-PAH fusion proteins were transfected in HeLa cells and experiments were started 18 h after transfection. To evaluate BH4 responsiveness, transfected cells were treated with 60 μM BH4 in aqueous solution. Analyses were performed 6 h later. Number and brightness (N&B) analysis was performed according to Gratton and colleagues [37,38] using a Zeiss LSM 510 META confocal microscope. Cells grown for 4 days on bottom glass dishes were imaged in vivo in CO_2-independent medium (150 mM NaCl, 5 mM KCl, 1 mM $CaCl_2$, 1 mM $MgCl_2$, and 20 mM Hepes, pH 7.4). Fifty frame time series were acquired with a LSM 510 META equipped with a plan apo 63× oil-immersion (NA 1.4) objective lens using the following settings: 488 nm Argon laser, 25% of output power, 1.5% transmission, 505–550 nm emission, gain equal to 850, offset 0.1, and digital gain 1. Scanning parameters were: 512 × 512 frame window, 25.61 μs/pixel dwell time, no average, zoom 6×, ROI (x,y) 256 × 64, and pinhole corresponding to 1 μm optical slice. Data from each cell were analyzed with the simFCS software (Globals Software, East Villa Grove, IL 61956, USA). Briefly, data analysis was performed pixel-by-pixel over time to calculate variance and average intensity. Correction was applied to take into account the analog detection of fluorescence by the photomultiplier tubes of the confocal microscope. Briefly, the correction parameters S, offset and sigma0 were determined, for each experiment, by plotting the measured average intensity (<I>) vs average variance (<Var>) of 50 frame time series acquired using same settings as above, but setting 4 different values of laser transmission percentages. Moreover, filters and beam splitters were configured to obtain reflection images to detect the defined amount of light originating directly from the laser. The obtained plots were linearly interpolated and the equation of straight line ($R \geq 0.99$) was used to extract the parameters S and offset based on the following equation: $<Var> = S * <I> + offset * S$. The parameter sigma0 was estimated from time-series acquired with laser off, as the half maximum width of the histogram peak of the "dark"-counts. Its value was constantly lower than 0.1, and consequently was approximated to zero in all the calculations. Brightness (B) was calculated pixel by pixel from the following equation $B = V(x,y)/(S * Ix,y)$, where I = Im-offset (Im: measured average fluorescence).

The number of molecule subunits constituting each oligomer was calculated with the following calibration procedure: the brightness of monomeric GFP and of GFP-based molecules made by two or three GFP moieties fused in tandem in expression vector pcDNA3.1 and expressed in HeLa cells were measured with the same experimental settings described above. The measured B values for monomeric, dimeric and trimeric GFP and the corresponding number of subunits were linearly interpolated to obtain the experimental equation describing the dependence of brightness on the number of GFP subunits: $B = k \times nsub + c$. This equation was used to calculate the unknown number of GFP subunits corresponding to the measured brightness. The following formula $B = sum(B_i^2\ n_i)/sum(B_i\ n_i)$ provides the brightness of multiple species (B_i) whose number is n_i in a single pixel, is combined in the measured brightness (B). This formula is used to interpret non integer subunit values obtained by the above procedure.

2.10. Structural analysis

The effect of the mutations on the 3D structure was investigated by analyzing the structural environment of each substituted residue in the PAH crystal structures deposited in the Protein Data Bank (PDB). Since no crystal structure of any full-length enzyme is available, various models were used: tetrameric human PAH lacking residues 1–117 (pdbcode 2pah); dimeric truncated human PAH lacking residues 1–117 and 425–452 (PDB code 1kw0); and the dimeric rat PAH, from residue 19 to 427 (pdbcode 1phz), which encompasses the regulatory domain. A composite monomeric model that included the three domains was built by superimposing the secondary structure elements of the respective catalytic domains of the rat (1phz) and human structures (2pah and 1kw0). The structural superposition was performed using the program O [39].

3. Results

3.1. Enzymatic activity analysis of wild-type and mutant forms of PAH

We measured the enzymatic activity of the equilibrium mixture of the wild-type and mutant forms of PAH to investigate the effect of the mutations on catalytic activity. As shown in Fig. 2, the residual activities of the mutant PAH enzymes, expressed as a percentage of wild-type enzyme activity, were: 38 ± 3% (p.I65M), 48 ± 14% (p.N223Y), 60 ± 12% (p.R297L), 69 ± 11% (p.F382L), 58 ± 9% (p.K398N), 43 ± 4% (p.A403V) and 63 ± 5% (p.Q419R). In our conditions, we found in multiple experiments that isolated oligomeric species are not stable and evolve toward the equilibrium mixture (see

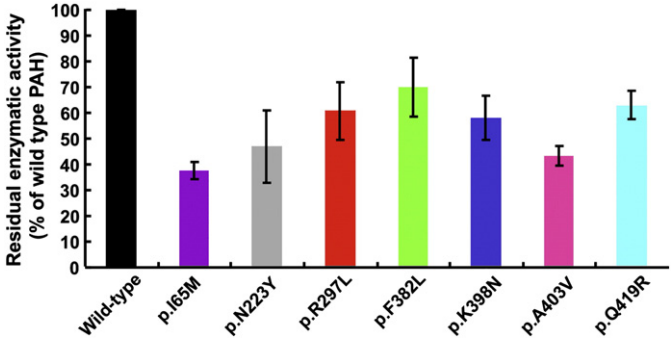

Fig. 2. Enzymatic activity of the PAH mutants expressed as percentage of wild-type PAH activity. The activity was measured by the amount of [^{14}C] Tyr produced by [^{14}C] Phe as analyzed by thin layer chromatography. Mean values and the standard deviation derived from three sets of independent experiments for each construct are shown expressed as percentage of wild-type PAH activity. The experimental assay conditions are reported in Section 2.4.

also below under Section 3.2); hence the activity of the isolated tetramers and dimers was not possible to be measured with accuracy.

3.2. Oligomerization equilibrium of wild-type and mutant forms of PAH

The oligomerization equilibrium for the fused MBP-PAH protein, the purified cleaved wild-type protein, and the missense mutants was analyzed by SEC (Fig. 3a,b). SEC runs were carried out at both 4 °C and room temperature. The elution profile was essentially the same at both temperatures, therefore only the data at room temperature are reported. Unless specified otherwise, SEC measurements were carried at a constant pH of 7.4 (buffer A). The SEC profiles revealed that wild-type and most of the mutant forms of PAH elute as tetramers and dimers although monomers and aggregates are also present, depending on the mutation of the protein. Fig. 3a shows the SEC profiles of proteins in which the tetramer is the most abundant species, i.e., the fused protein, the cleaved wild-type PAH and mutant p.R297L. Fig. 3b shows the profiles of the wild-type PAH (as reference) and of mutants p.I65M, p.N223Y, p.F382L, p.K398N, p.A403V and p.Q419R in which dimer is the dominant species. The peaks corresponding to tetramer, dimer and monomer species elute at 11.5 mL, 13.1 mL and 14.7 mL respectively (Fig. 3a,b).

The presence of the PAH protein was confirmed in each of the fractions obtained by SEC (Fig. 3a) after separation by SDS/PAGE and Western blot analysis using anti-PAH serum (Fig. 3c). This result demonstrates the existence of a monomeric form of the PAH enzyme. This form was probably underestimated in previous studies because it was masked by MBP. Western blot analysis also showed that samples did not contain MBP after cleavage (Fig. 3c).

The percentage of PAH oligomeric species is reported in Fig. 4 (see also Supplementary Table S1). The tetramer and dimer species of the wild-type PAH were separately collected and stored for less than one week at 4 °C. Subsequently, SEC analysis of tetramers and dimers showed that the tetramer shifts back toward the dimer and the monomer, while the dimer is fairly stable, since about 90% of the protein applied was recovered in the dimeric form (data not shown), according to literature data [21].

All chromatographic runs were done in conjunction with MALS. The masses resulting from MALS measurements in wild-type PAH mutants were 203 kDa (within 1%) and 102 kDa (within 3%) for tetramer species and dimer species, respectively. Because of the small quantities of monomer, we were not able to calculate its molecular mass. A representative profile of wild-type PAH obtained from MALS is shown in Fig. 5.

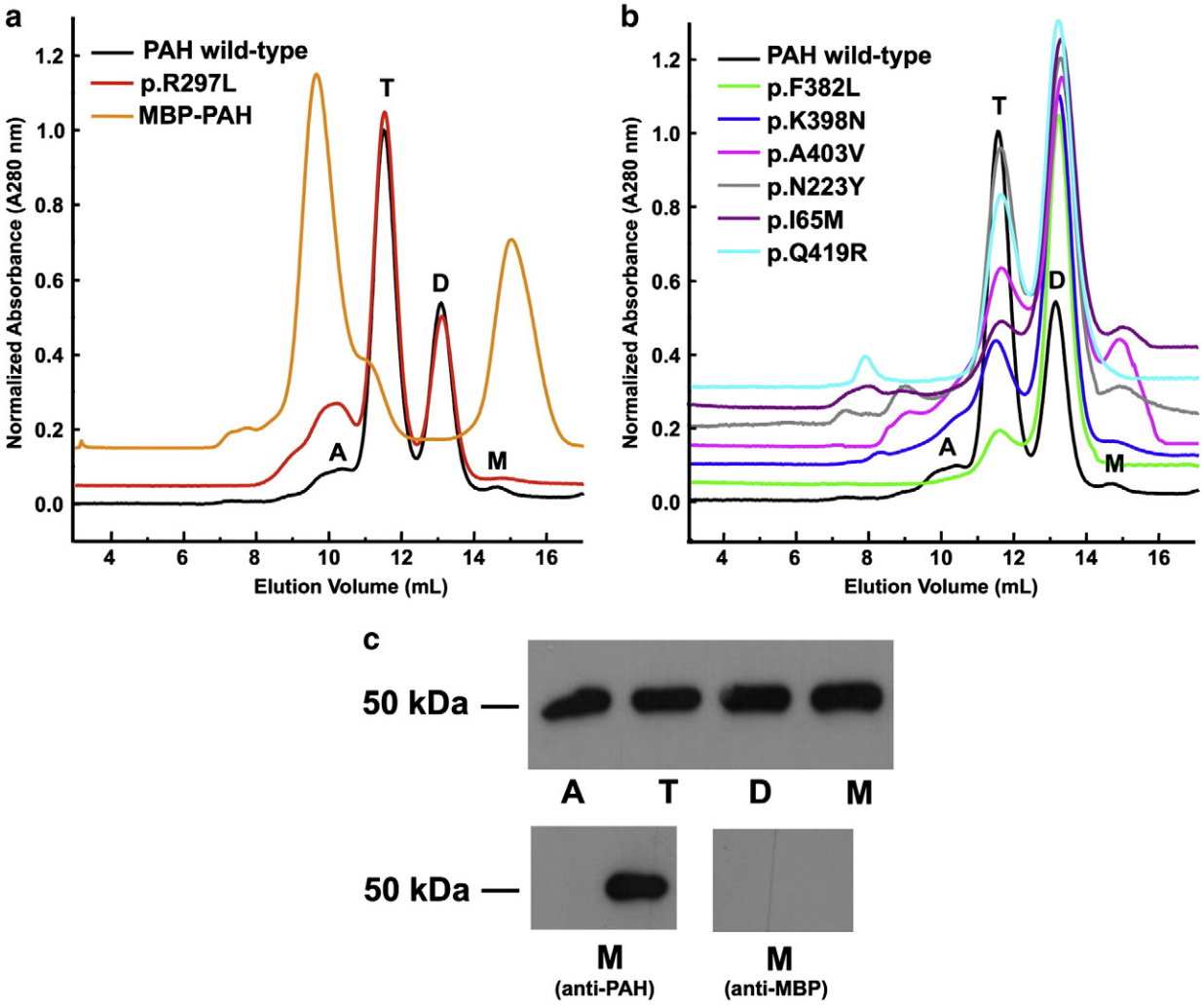

Fig. 3. Chromatographic profiles of the PAH natural variants and immunoblotting of wild-type PAH. a) Size exclusion chromatographic (SEC) runs carried out in buffer A (see text) and normalized in the 0.0 ÷ 1.2 interval. All curves are shifted along the ordinate axis by 0.05n, n integer ($1 \le n \le 5$), with respect to the wild-type PAH curve. b) SEC runs of wild-type and other mutant recombinant PAH proteins. All curves are shifted along the ordinate axis by 0.05n, n integer ($1 \le n \le 5$), with respect to the wild-type PAH curve, to better visualize the single curves. c) Western blot analysis using the anti-PAH antibody of each of the fractions in panel a obtained from wild-type (depicted as a black curve in a); peak A) aggregated forms, possibly multimeric; peak T) tetramer; peak D) dimer; peak M) monomer. Western blot analysis of the wild-type PAH monomer (peak M of panel a) with anti-PAH or anti-MBP antibodies.

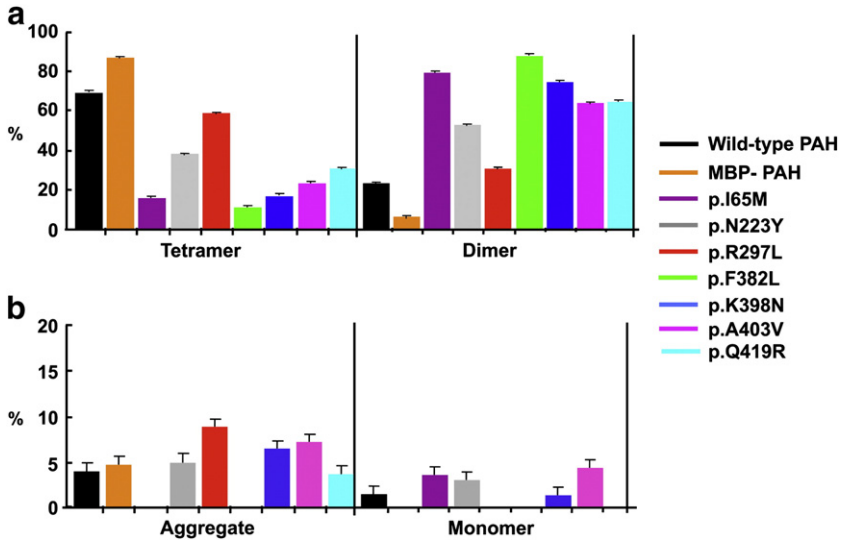

Fig. 4. Percentage of the molecular species of the recombinant wild-type PAH protein and its mutants. The histograms indicate a) the percentage of tetramers and dimers, and b) the percentage of aggregate and monomers of recombinant wild-type PAH, MBP-PAH, p.I65M, p.N223Y, p.R297L, p.F382L, p.K398N, p.A403V and p.Q419R. All data with standard deviations were calculated on at least triplicate runs carried out at 20 °C.

3.3. Thermal stability and inactivation

The dominant oligomeric species of wild-type PAH and mutants, collected after gel filtration and dialyzed against buffer C, were analyzed by CD. The CD spectra of all samples were recorded in the far-UV region (190–250 nm), in buffer C, pH 7.4, at 20 °C. Fig. 6a shows the normalized spectra for wild-type PAH and selected mutants, together with the spectrum for the fused wild-type MBP-PAH. In the spectra of Fig. 6a, the maximum centered at 195 nm and the two broad minima centered at 208 and 222 nm are indicative of the presence of both α and β secondary structure elements. The spectra profiles do not differ significantly from each other, but the molar ellipticity of all the mutants is much lower than that of wild-type enzyme. Therefore, these spectra provide evidence for local unfolding of the mutants.

We also recorded the thermal denaturation curves in the 20÷80 °C temperature range by monitoring the molar ellipticity at 222 nm (Fig. 6b) of the most abundant oligomeric species of cleaved PAH proteins (Figs. 3a,b; 4, Supplementary Table S1). The far-UV CD spectra of denatured species of all samples at 80 °C are typical of random coil (data not shown). The spectrum of cooled samples after denaturation is virtually identical to that of the denatured protein at 80 °C (data not shown), thereby confirming the irreversibility of the unfolding process, as previously reported [24,40]. In the case of the wild-type PAH, the denaturation curve of the equilibrium mixture was also recorded; for comparison purposes, this curve and that of the tetramer are shown in Fig. 6c. It is clear that the denaturation process depends on the oligomeric species.

The sigmoidal denaturation curve obtained with the fused wild-type MBP-PAH protein shows two inflection points, with a plateau, corresponding to the two melting temperatures of the two proteins. Visual inspection of the denaturation curves (Fig. 6b) of the cleaved PAH proteins shows a sigmoidal shape with a single inflection point. Differently, a detailed analysis of the curves through the first derivatives, revealed two midpoints corresponding to two transitions (data not shown), according to literature data [40]. As shown in Table 2, the melting temperatures of the PAH proteins range from 33 to 57 °C. The thermal denaturation curve of mutant p.F382L is significantly shifted to lower temperatures with respect to the wild-type PAH (Fig. 6b). Therefore, we carried out the thermal inactivation assay of the wild-type PAH and the p.F382L mutant at temperatures between 32 and 58 °C (Fig. 6d). Consistently, the p.F382L mutant was much more temperature sensitive than the wild-type enzyme. In fact, under these conditions a lower amount of Tyr was produced (Fig. 6d), and the half-inactivation temperature was close to 44 °C, which well agrees with the value of $T_{m2} = 43.6$ °C obtained by CD. These findings show that the stability of specific mutants, such as p.F382L, can markedly diverge from that of the wild-type protein.

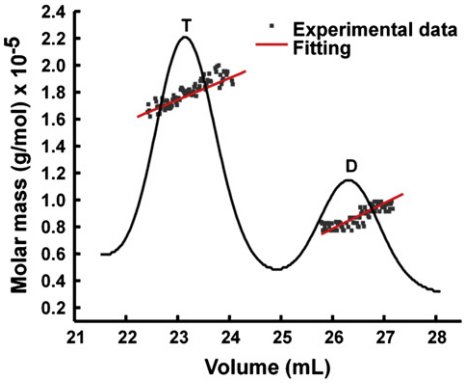

Fig. 5. SEC-MALS analysis of wild-type PAH. Representative profile of wild-type PAH obtained from light scattering and refractive index detectors. The molecular mass is shown. The experimental data are represented by squares and the fitting of experimental data is shown by a red line.

3.4. N&B analysis

Confocal microscopy observation of cells expressing GFP-wild-type PAH and GFP-A403V fusion proteins revealed a cytoplasmic localization of PAH and its mutant p.A403V, as expected (Fig. 7a,b). No fluorescence was detected in the cell nuclei. To estimate the number of subunits constituting wild-type PAH and the p.A403V mutant at steady state in live cells, the recently developed N&B technique was performed on cells expressing the fusion proteins treated and not with BH4 for 6 h. The "brightness" of the GFP-wild-type PAH fusion protein was 1.091 and 1.099 upon BH4 treatment, which, at the t-test, was not significantly different from values obtained without BH4 treatment. On the contrary, in cells expressing the GFP-A403V fusion protein there was a statistically significant ($p<0.001$) shift of brightness from 1.047 without BH4 to 1.094 upon its addition.

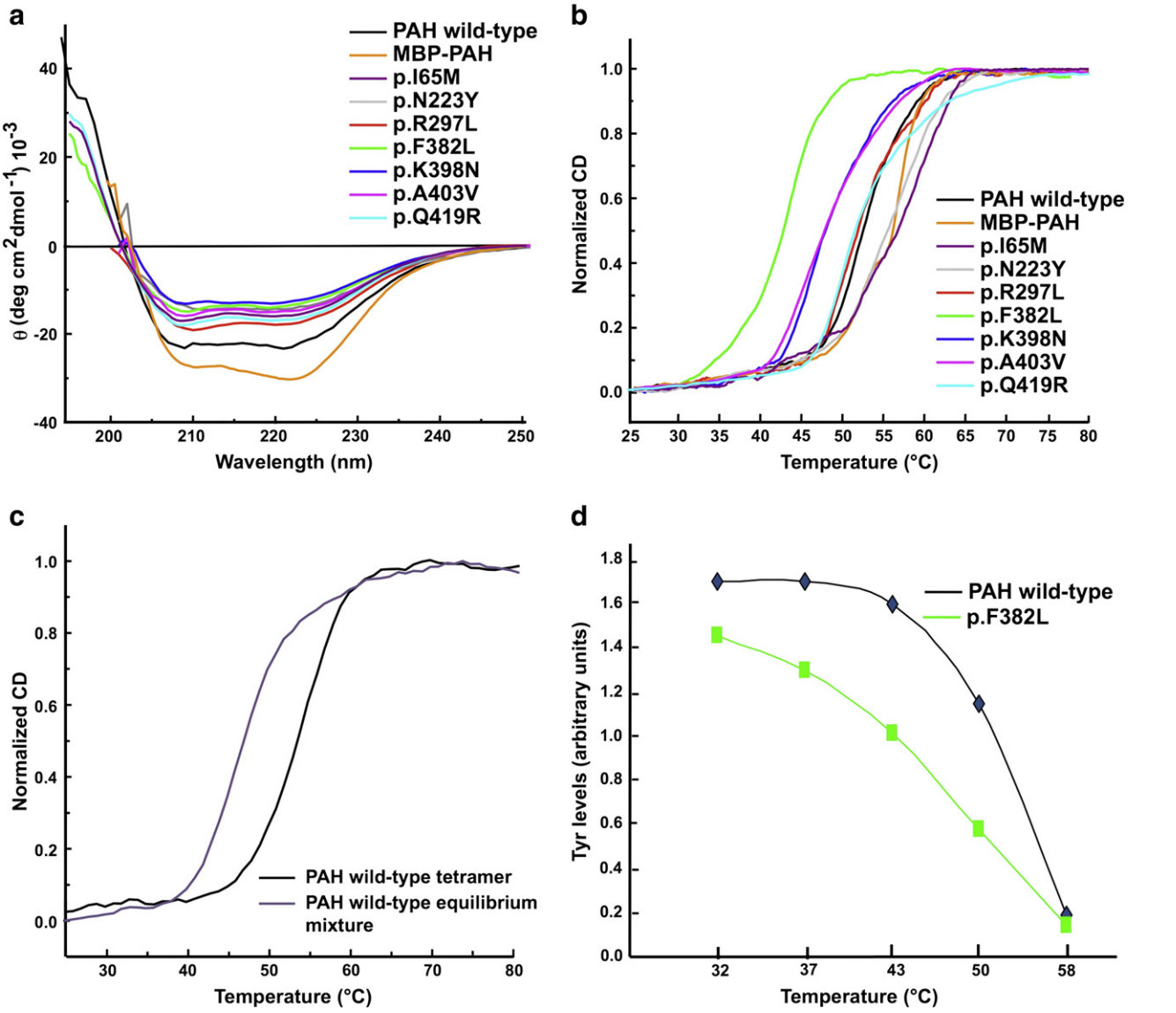

Fig. 6. CD measurements. a) Far-UV spectra recorded in buffer C (see text) at 20 °C. b) CD-monitored thermal unfolding curves in the 25–80 °C temperature range. The change of the molar ellipticity at 222 nm was monitored versus the temperature. The most abundant oligomeric form was considered for each PAH protein. c) Thermal denaturation of the tetrameric form and of the equilibrium mixture of cleaved wild-type PAH. d) Thermal inactivation assay of wild-type and F382L PAH. Proteins were incubated at increasing temperatures and the amount of produced tyrosine was determined.

These brightness values were used to calculate the number of subunits that constitute each PAH oligomer at steady state, namely wild-type and p.A403V before and after BH4 administration (see Material and methods for details). Briefly, a calibration curve (number of subunits vs brightness) was constructed using reference GFP-based molecules constituted by 1, 2 or 3 GFP monomers and measuring their brightness in the same experimental conditions used above. The reference curve obtained (which was perfectly linear) was used to extrapolate the unknown number of subunits from the brightness of GFP-PAHs. The wild-type PAH conserved an average number of subunits (see Material and methods for definition of "average number of subunits") equal to approximately 3.1, which reflects the presence of tetramers and dimers in equilibrium. The addition of BH4 did not affect this number. Differently, exposure of the A403V-PAH mutant form to BH4 caused the subunit number to increase from 2.4 to 3.1, this latter being the same as that of the wild-type enzyme (Fig. 7c).

Table 2
Melting temperatures inferred by first derivative of unfolding curves.[a]

Forms of PAH	$T_{m1} \pm 1.0$ (°C)	$T_{m2} \pm 1.0$ (°C)
Wild-type PAH	52.2	57.6
MBP-PAH	52.0	57.5
p. I65M	53.0	59.2
p.N223Y	54.2	57.6
p.R297L	50.8	59.0
p.F382L	32.6	43.6
p.K398N	46.4	53.6
p.A403V	46.0	55.6
p.Q419R	50.1	57.3

All experiments were conducted in buffer C (see Material and methods).
[a] See also Fig. 6b.

4. Discussion

4.1. The oligomerization equilibrium is shifted toward the dimeric form in PAH mutants

To characterize the oligomeric state of PAH in solution, we performed SEC with on-line detection of LS and refractive index signals. This approach allowed us to measure the molecular mass of

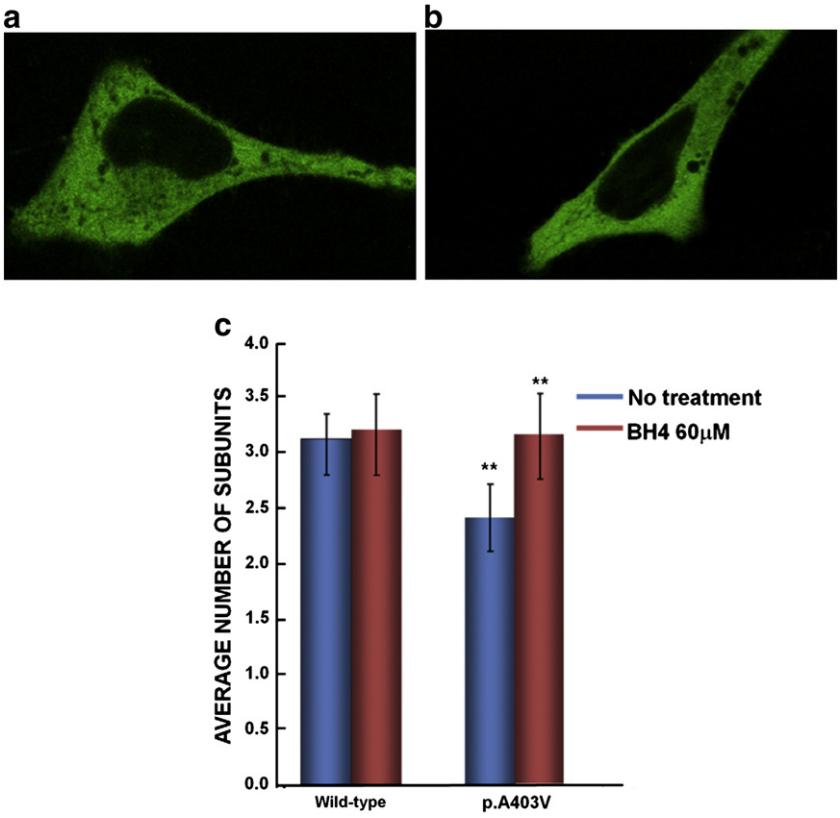

Fig. 7. N&B analysis. a) Confocal microscopy images of cells expressing GFP-wild-type PAH protein and b) GFP-p.A403V mutant protein. c) Histograms showing the oligomeric state of both GFP-wild-type PAH and GFP-p.A403V mutant in untreated (blue bars) and BH4-treated (red bars) cells. Asterisks above the bars indicate statistical significance for the p.A403V mutant protein.

the eluted peaks independently of their shape and/or amino acid composition and elution volume. The operative conditions used in the SEC experiments were the same for all samples. No substrate, cofactor or any other compound was added and only a buffer at physiological pH (buffer A; pH 7.4) was used because a lower pH and the addition of L-Phe can affect the oligomeric equilibrium [10].

In line with previous data [10,21,24], the SEC profile of the fused wild-type MBP-PAH protein revealed that tetramer was the dominant species (88.4%), whereas the dimeric form was less abundant and the monomeric form was absent. Differently, all three species were obtained in the cleaved full-length wild-type enzyme (see Fig. 4 and Supplementary Table S1 for the relative percentages). The observation of three distinct peaks demonstrates that self-association of monomers or dimers is slow on the time scale of separation. Previous studies showed that both fused and truncated/cleaved forms of wild-type and mutant enzymes consist of an equilibrium mixture of dimeric and tetrameric species in a ratio that depends on the protein nature and on the experimental conditions used [10,24].

Only in a few cases in which proteins were expressed in a coupled in vitro transcription–translation eukaryotic system [41,42] was the monomeric form also detected. Here, we report evidence that a monomer species occurs in the equilibrium mixture of PAH albeit in a low amount. The presence of a monomer species may have been underestimated in previous studies for several reasons: i) because of its low abundance, ii) because the fused protein was analyzed [24] or iii) because the cleaved wild-type PAH was analyzed in the presence of MBP which co-elutes with the PAH monomer [10]. Western blot analysis (Fig. 3c) and re-chromatography of the isolated tetramer of wild-type PAH, which regenerate the dimer and the monomer peak (data not shown), indicate that the monomer contributes to the equilibrium mixture. The equilibrium mixture of the PAH enzyme can be described as follows: $4M \leftrightarrows 2D \leftrightarrows T$.

The oligomerization process of the mutants is clearly disturbed by the mutation, except in the case of mutant p.R297L that has a SEC profile similar to that of the wild-type enzyme although it lacks a monomer (Fig. 3a). For all the other mutants (p.I65M, p.N223Y, p.F382L, p.K398N, p.A403V and p.Q419R), the equilibrium was shifted toward the dimeric enzyme (Fig. 3b). In any event, all mutants present a reduced activity of the enzyme because of the diverse composition of the equilibrium mixture. This confirms that oligomerization defects of PAH variants are one of the most common causes of HPAs.

4.2. Thermal stability and defect at the secondary structure level of PAH mutants

The CD spectrum of wild-type PAH is characterized by typical fingerprints of α/β proteins (Fig. 6a), in line with the known 3D structure [43]. Despite the similarity of CD spectra profiles in the wild-type and mutant forms of PAH, the latter present a partial loss of secondary structure with respect the wild-type folded structure, their molar ellipticity being significantly decreased (Fig. 6a). This loss occurs for all the mutants except for mutant p.R297L in which the loss is less pronounced. Therefore, the CD spectra have provided evidence for a folding defect at secondary structure level. To characterize further all the PAH mutants, we estimated the α-helical content using the equation of Richardson and Makhatadze [44]. The calculations showed a progressive decrease of the α-helical content of the PAH mutants (see Supplementary Table S2).

Thermal denaturation of all the PAH proteins proved to be an irreversible process as previously reported [40]. Therefore, the thermodynamic features of the enzyme cannot be further characterized. As expected for the wild-type MBP-PAH fused protein, the two steps in the sigmoidal curve correspond to two independent unfolding processes for the two proteins. Indeed, the two melting

temperatures (Table 2) correspond to the independent structural collapse of PAH (52.0 °C) and MBP (57.5 °C), respectively (see also Supplementary data for details).

Earlier differential scanning calorimetry, fluorescence and CD experiments indicated that, upon heating, two partially overlapping transitions occur with an apparent melting temperature T_{m1} of about 46 °C and a T_{m2} of about 54 °C, respectively [14,40]. Apart from rare exceptions, two transitions were identified also in the mutants. Their melting temperatures diverged from that of wild-type PAH within a range from −6 to +2 °C [24,45]. On the other hand, unfolding experiments conducted on the truncated PAH (aa 112–452) revealed only one cooperative transition centered at about 54 °C [40]. Therefore, the first transition was interpreted as a denaturation of the N-terminal regulatory domain and the second, partially overlapping transition as a denaturation of the catalytic-tetramerization domain [40].

Unfolding experiments were carried out for wild-type PAH and mutants in buffer C and the ellipticity at 222 nm was monitored as a function of temperature. Two overlapping transitions occurred for the wild-type PAH and all the mutants. For the wild-type PAH, the T_{m1} and T_{m2} were 52.2 °C and 57.6 °C, slightly different from previous reports [24,40,45]. This discrepancy is due to the species studied. If the denaturation process is followed using only the PAH tetramer, as in our case, the melting temperatures are $T_{m1} = 52.2$ °C and $T_{m2} = 57.6$ °C. On the other hand, if all the species present in the oligomerization equilibrium are considered, the T_{m1} well agrees with that reported previously ($T_{m1} = 46.1$ °C) (Fig. 6c) [24,40,45]. To verify that the unfolding process depends only on the oligomerization equilibrium, we carried out unfolding experiments in the same buffer and scan-rate conditions used in previous studies (buffer B, scan-rate 0.7 °C/min) [40,45], and obtained a T_{m1} and T_{m2} of 52.0 °C and 54.8 °C, respectively. Indeed, a small destabilization has been reported for most of the previously described mutants, as shown by a decrease in ΔT_m of about a couple of degrees. There are only a few instances where ΔT_m decreases down to ~6 °C [45]. For example, T_{m1} and T_{m2} decreased by as much as 42.6 °C and 52.0 °C and 40.7 °C and 50.2 °C, respectively in the non-natural mutants p.N223D and p.T427P with respect to wild-type enzyme T_{m1} and T_{m2} [45].

The melting temperatures of mutants p.I65M and p.N223Y indicate a very marginal stability gain, being only a couple of degrees higher with respect to the wild-type enzyme (Table 2). Furthermore, the denaturation curves of p.R297L and p.Q419R are similar, and the denaturation slopes differ only slightly from that of the wild-type enzyme, which indicates that the thermal stability is hardly affected. For mutants p.K398N and p.A403V, however, the T_{m1} is about 6° lower and the T_{m2} about 2–3° lower with respect to the wild-type, thereby indicating a loss of stability. Interestingly, the T_{m1} (33.0 °C) and T_{m2} (43.6 °C) of mutant p.F382L are about 20 °C and 14 °C lower with respect to those of the wild-type enzyme, which indicates that this enzyme variant has a high thermal structural instability.

The results of thermal denaturation experiments of the p.F382L mutant suggest that the replacement of L-Phe by L-Leu at position 382 leads to temperature-dependent functional alterations. These results were confirmed by the thermal inactivation assay performed on the p.F382L mutant and, for comparison, on the wild-type PAH. Indeed, the half-inactivation temperature obtained for this mutant (~44 °C) well agrees with the T_{m2} of 43.6 °C obtained by CD (Fig. 6b and d, Table 2).

4.3. Mapping the mutations to search for structural alterations

For the present study, we built a composite model of the full-length human enzyme and used it as a template for structural analysis of the wild-type and mutant proteins. Mutations p.I65M and p.Q419R fall in the regulatory and tetramerization domain, respectively; mutations p.N223Y, p.R297L, p.F382L, p.K398N and p.A403V fall in the large catalytic domain. All mutations are far from the active and cofactor binding sites. All, except mutations at positions 65 and 403, are located on the surface of the molecule in hydrated regions. In Fig. 1, the position of the seven mutations is drawn on the monomer structure. There are four previously identified variants at codon 65 (p.I65T, p.I65V, p.I65N, and p.I65S). The PAH database contains in vitro expression data only for p.I65T, namely, increased proteolytic degradation in pulse-chase experiments, increased aggregation and decreased solubility. The residual activity of the I65T/V mutants, tested in different in vitro systems, was about 21–29% (http://www.pahdb.mcgill.ca).

Ile65 is located in a hydrophobic environment of the regulatory domain. In the mutant enzyme p.I65M, the Ile change to a somewhat larger but differently shaped Met may distort the hydrophobic packing of the region [30]. In addition, Ile 65 makes a favorable interaction with the catalytic domain of another subunit within the dimer (the Ile65 oxygen atom is hydrogen-bonded to the hydroxyl group of Tyr 216). As a result, both the tertiary structure and the quaternary structure are perturbed. These data are in line with the dimer abundance (Fig. 4 and Supplementary Table S1).

Asn223 is located in a solvent exposed loop [46]. In mutant p.N223Y the structural perturbation is mainly due to tyrosine solvent exposure that may affect the function. It has been proposed that this residue is embodied in an intra-domain hinge bending region [45] that is involved in the conformational transition induced by substrate binding. Overall, its properties are similar to those of the wild-type enzyme, except that the dimeric form is favored over the tetramer. Mutant p.R297L exhibits properties very similar to those of the wild-type enzyme. Interestingly, two other mutants reported in the database, i.e., p.R297C and p.R297H, which are also associated with a mild phenotype, indicate that mutations at this site are not critical [32].

Mutant p.F382L is the one that differs most from the wild-type enzyme. It occurs prevalently as a dimer (88.3%). Moreover, the mutation falls in a region rich in aromatic residues. L-Phe forms various stacking aromatic interactions with the aromatic residues Tyr356 and Tyr277 in the wild-type enzyme [33]. The replacement by Leu, despite the hydrophobic nature of this residue, breaks the aromatic network and results in marked destabilization. This is in line with larger ΔT_{m1} (19.6 °C) and ΔT_{m2} (14.0 °C) and with a lower inactivation temperature compared to the wild-type protein (Fig. 6d). This is the largest difference observed so far for a PAH mutant. This highlights that L-Phe in position 382 is crucial for the stability of this aromatic amino acid-rich region.

Lys398 is located at the tetramer interface, although it is not directly engaged in intersubunit interactions. The positively charged Lys is embedded in a negatively charged environment because of the presence of Asp394 and Glu390 [43]. The high dimer/tetramer ratio observed for mutant pK398N (75.0/17.2, Fig. 4 and Supplementary Table S1) is in line with tetramer destabilization. Also the structural stability was decreased. In fact, T_{m1} and T_{m2} were lower than that of the wild-type enzyme being 5.6 and 4.0 °C, respectively (Table 2). Q419 lies in a hydrated region at the dimer/tetramer interface. The substitution of Gln by an Arg generates unfavorable ionic interactions with a nearby Arg241 that destabilize the tetramer. The thermal stability of p.Q419R is not significantly affected by the mutation.

4.4. BH4 effect and the dimer–tetramer p.A403V equilibrium

In this study, we investigated the effect of BH4 on p.A403V that, in our geographic area, is the most frequent mutant in mild, BH4-responsive patients [32,33]. To this aim, we used the N&B technique that has been successfully employed to discern minor changes in molecular composition [37,38]. We monitored the fluorescent molecular forms of GFP-wild-type PAH and the GFP-A403V mutant after transient transfection of HeLa cells. The addition of BH4 to the

wild-type enzyme did not cause any change. Differently, BH4 addition to cells expressing the p.A403V mutant promoted a shift from dimeric to tetrameric molecular forms.

The BH4 responsiveness in HPA has been the subject of numerous studies. Various mechanisms have been proposed to explain BH4-responsiveness, namely: increased enzyme activity [1,30,47,48], correction or compensation of the BH4 decreased affinity, protection toward catalytic inactivation and chaperone-like activity that, by stabilizing the protein, protects it from proteolytic degradation [1,15,30]. In addition, BH4 supplementation may restore the optimal concentration of BH4 cofactor in hepatocytes [28,46]. In our study, the N&B technique revealed that the addition of BH4 to HeLa living cells influences the oligomerization equilibrium of the p.A403V mutant by shifting it toward a tetrameric quaternary structure.

4.5. Concluding remarks

About 600 mutations associated with the PKU/HPA phenotype have been identified in the PAH gene. The resulting phenotypes range from mild to severe HPA. This study demonstrates that our seven gene variants reduce the enzymatic activity to 38–69% of that of wild-type activity and affect the oligomerization state, thermal stability and folding of PAH protein. Perturbation of these biophysical and biochemical features may, therefore, be considered major disease-causing alterations, also in mild phenotypic forms of HPAs. In addition to the well recognized effect of BH4 on the stability of PAH mutants [30], we provide the first evidence, obtained with the N&B technique, that in cellulo exposure to BH4 influences the oligomerization equilibrium of the p.A403V mutant. Therefore, we surmise that, in this case, a shift from dimer to tetramer plays a major role in BH4 responsiveness.

Acknowledgements

This study was supported by grants from Regione Campania (Convenzione CEINGE-Regione Campania, G.R. 27/12/2007), from Ministero dell'Istruzione, dell'Università e della Ricerca-Rome PS35-126/IND, from IRCCS – Fondazione SDN, and from Ministero Salute, Rome, Italy.

We thank Simona Monti and Nina Dathan for their suggestions and advices regarding SEC. Pompea del Vecchio and Vincenzo Granata are acknowledged for their comments regarding CD measurements. We are grateful to Jean Ann Gilder (Scientific Communication srl) for revising and editing the text, and to Vittorio Lucignano for graphic editorial help in figure composition.

Appendix A. Supplementary data

Supplementary data to this article can be found online at doi:10.1016/j.bbadis.2011.07.012.

References

[1] C.R. Scriver, The PAH gene, phenylketonuria, and a paradigm shift, Hum. Mutat. 28 (2007) 831–845.
[2] N. Blau, B. Thony, R.G.H. Cotton, K. Hyland, Disorders of tetrahydrobiopterin and related biogenic amines, in: C.R. Scriver, A.L. Beaudet, W.S. Sly, D. Valle, B. Vogelstein (Eds.), The Metabolic and Molecular Bases of Inherited Disease, McGraw_Hill, New York, 2001, pp. 1725–1776.
[3] R.A. Williams, C.D. Mamotte, J.R. Burnett, Phenylketonuria: an inborn error of phenylalanine metabolism, Clin. Biochem. Rev. 29 (2008) 31–41.
[4] M. Giovannini, E. Verduci, E. Salvatici, L. Fiori, E. Riva, Phenylketonuria: dietary and therapeutic challenges, J. Inherit. Metab. Dis. 30 (2007) 145–152.
[5] H.L. Levy, A. Milanowski, A. Chakrapani, M. Cleary, P. Lee, F.K. Trefz, C.B. Whitley, F. Feillet, A.S. Feigenbaum, J.D. Bebchuk, H. Christ-Schmidt, A. Dorenbaum, Efficacy of sapropterin dihydrochloride (tetrahydrobiopterin, 6R-BH4) for reduction of phenylalanine concentration in patients with phenylketonuria: a phase III randomised placebo-controlled study, Lancet 370 (2007) 504–510.
[6] M. Cerreto, R. Nistico, D. Ombrone, M. Ruoppolo, A. Usiello, A. Daniele, L. Pastore, F. Salvatore, Complete reversal of metabolic and neurological symptoms in PKU mice after PAH-HD-Ad vector treatment, Hum. Gene Ther. 11 (2009) 1391.
[7] F.J. Van Spronsen, G.M. Enns, Future treatment strategies in phenylketonuria, Mol. Genet. Metab. 99 (2010) 90–95.
[8] F. Fusetti, H. Erlandsen, T. Flatmark, R.C. Stevens, Structure of tetrameric human phenylalanine hydroxylase and its implications for phenylketonuria, J. Biol. Chem. 273 (1998) 16962–16967.
[9] A.P. Doskeland, A. Martinez, P.M. Knappskog, T. Flatmark, Phosphorylation of recombinant human phenylalanine hydroxylase: effect on catalytic activity, substrate activation and protection against non-specific cleavage of the fusion protein by restriction protease, Biochem. J. 313 (1996) 409–414.
[10] A. Martinez, P.M. Knappskog, S. Olafsdottir, A.P. Doskeland, H.G. Eiken, R.M. Svebak, M. Bozzini, J. Apold, T. Flatmark, Expression of recombinant human phenylalanine hydroxylase as fusion protein in *Escherichia coli* circumvents proteolytic degradation by host cell proteases. Isolation and characterization of the wild-type enzyme, Biochem. J. 306 (Pt 2) (1995) 589–597.
[11] S. Kaufman, The phenylalanine hydroxylating system, Adv. Enzymol. Relat. Areas Mol. Biol. 67 (1993) 77–264.
[12] O.A. Andersen, A.J. Stokka, T. Flatmark, E. Hough, 2.0 Å resolution crystal structures of the ternary complexes of human phenylalanine hydroxylase catalytic domain with tetrahydrobiopterin and 3-(2-thienyl)-L-alanine or L-norleucine: substrate specificity and molecular motions related to substrate binding, J. Mol. Biol. 333 (2003) 747–757.
[13] A. Doskeland, T. Ljones, T. Skotland, T. Flatmark, Phenylalanine 4-monooxygenase from bovine and rat liver: some physical and chemical properties, Neurochem. Res. 7 (1982) 407–421.
[14] F.F. Miranda, M. Thòròlfsson, K. Teigen, J.M. Sanchez-Ruiz, A. Martinez, Structural and stability effects of phosphorylation: localized structural changes in phenylalanine hydroxylase, Protein Sci. 13 (2004) 1219–1226.
[15] C.R. Scriver, P.J. Waters, Monogenic traits are not simple: lessons from phenylketonuria, Trends Genet. 15 (1999) 267–272.
[16] S. Giannattasio, I. Dianzani, P. Lattanzio, M. Spada, V. Romano, F. Cali, G. Andria, A. Ponzone, E. Marra, A. Piazza, Genetic heterogeneity in five Italian regions: analysis of PAH mutations and minihaplotypes, Hum. Hered. 52 (2001) 154–159.
[17] P. Guldberg, F. Rey, J. Zschocke, V. Romano, B. Francois, L. Michiels, K. Ullrich, G.F. Hoffmann, P. Burgard, H. Schmidt, C. Meli, E. Riva, I. Dianzani, A. Ponzone, J. Rey, F. Guttler, A European multicenter study of phenylalanine hydroxylase deficiency: classification of 105 mutations and a general system for genotype-based prediction of metabolic phenotype, Am. J. Hum. Genet. 63 (1998) 71–79.
[18] J. Zschocke, Phenylketonuria mutations in Europe, Hum. Mutat. 21 (2003) 345–356.
[19] H.G. Eiken, P.M. Knappskog, J. Apold, T. Flatmark, PKU mutation G46S is associated with increased aggregation and degradation of the phenylalanine hydroxylase enzyme, Hum. Mutat. 7 (1996) 228–238.
[20] M. Thórólfsson, K. Teigen, A. Martinez, Activation of phenylalanine hydroxylase: effect of substitutions at Arg68 and Cys 237, Biochem. 42 (2003) 3419–3428.
[21] P.M. Knappskog, T. Flatmark, J.M. Aarden, J. Haavik, A. Martinez, Structure/function relationships in human phenylalanine hydroxylase. Effect of terminal deletions on the oligomerization, activation and cooperativity of substrate binding to the enzyme, Eur. J. Biochem. 242 (1996) 813–821.
[22] B. Kobe, I.G. Jennings, C.M. House, B.J. Michell, K.E. Goodwill, B.D. Santarsiero, R.C. Stevens, R.G. Cotton, B.E. Kemp, Structural basis of autoregulation of phenylalanine hydroxylase, Nat. Struct. Biol. 6 (1999) 442–448.
[23] P.J. Waters, M.A. Parniak, B.R. Akerman, A.O. Jones, C.R. Scriver, Missense mutations in the phenylalanine hydroxylase gene (PAH) can cause accelerated proteolytic turnover of PAH enzyme: a mechanism underlying phenylketonuria, J. Inherit. Metab. Dis. 22 (1999) 208–212.
[24] S.W. Gersting, K.F. Kemter, M. Staudigl, D.D. Messing, M.K. Danecka, F.B. Lagler, C.P. Sommerhoff, A.A. Roscher, A.C. Muntau, Loss of function in phenylketonuria is caused by impaired molecular motions and conformational instability, Am. J. Hum. Genet. 83 (2008) 5–17.
[25] T. Gjetting, M. Petersen, P. Guldberg, F. Guttler, In vitro expression of 34 naturally occurring mutant variants of phenylalanine hydroxylase: correlation with metabolic phenotypes and susceptibility toward protein aggregation, Mol. Genet. Metab. 72 (2001) 132–143.
[26] P.J. Waters, M.A. Parniak, B.R. Akerman, C.R. Scriver, Characterization of phenylketonuria missense substitutions, distant from the phenylalanine hydroxylase active site, illustrates a paradigm for mechanism and potential modulation of phenotype, Mol. Genet. Metab. 69 (2000) 101–110.
[27] A.L. Pey, F. Stricher, L. Serrano, A. Martinez, Predicted effects of missense mutations on native-state stability account for phenotypic outcome in phenylketonuria, a paradigm of misfolding diseases, Am. J. Hum. Genet. 81 (2007) 1006–1024.
[28] C. Aguado, B. Perez, M. Ugarte, L.R. Desviat, Analysis of the effect of tetrahydrobiopterin on PAH gene expression in hepatoma cells, FEBS Lett. 580 (2006) 1697–1701.
[29] M. Staudigl, S.W. Gersting, M.K. Danecka, D.D. Messing, M. Woidly, D. Pinkas, K.F. Kemter, N. Blau, A.C. Muntau, The interplay between genotype, metabolic state and cofactor treatment governs phenylalanine hydroxylase function and drug response, Hum. Mol. Genet. 20 (2011) 2628–2641.
[30] H. Erlandsen, A.L. Pey, A. Gamez, B. Perez, L.R. Desviat, C. Aguado, R. Koch, S. Surendran, S. Tyring, R. Matalon, C.R. Scriver, M. Ugarte, A. Martinez, R.C. Stevens, Correction of kinetic and stability defects by tetrahydrobiopterin in phenylketonuria patients with certain phenylalanine hydroxylase mutations, Proc. Natl. Acad. Sci. U. S. A. 101 (2004) 16903–16908.
[31] A.C. Muntau, S.W. Gersting, Phenylketonuria as a model for protein misfolding diseases and for the development of next generation orphan drugs for patients with inborn errors of metabolism, J. Inherit. Metab. Dis. 33 (2010) 649–658.

[32] A. Daniele, G. Cardillo, C. Pennino, M.T. Carbone, D. Scognamiglio, A. Correra, A. Pignero, G. Castaldo, F. Salvatore, Molecular epidemiology of phenylalanine hydroxylase deficiency in Southern Italy: a 96% detection rate with ten novel mutations, Ann. Hum. Genet. 71 (2007) 185–193.
[33] A. Daniele, G. Cardillo, C. Pennino, M.T. Carbone, D. Scognamiglio, L. Esposito, A. Correra, G. Castaldo, A. Zagari, F. Salvatore, Five human phenylalanine hydroxylase proteins identified in mild hyperphenylalaninemia patients are disease-causing variants, Biochim. Biophys. Acta. 1782 (2008) 378–384.
[34] A. Daniele, I. Scala, G. Cardillo, C. Pennino, C. Ungaro, M. Sibilio, G. Parenti, L. Esposito, A. Zagari, G. Andria, F. Salvatore, Functional and structural characterization of novel mutations and genotype–phenotype correlation in 51 phenylalanine hydroxylase deficient families from Southern Italy, FEBS J. 276 (2009) 2048–2059.
[35] T. Bardelli, M.A. Donati, S. Gasperini, F. Ciani, F. Belli, N. Blau, A. Morrone, E. Zammarchi, Two novel genetic lesions and a common BH4-responsive mutation of the PAH gene in Italian patients with hyperphenylalaninemia, Mol. Genet. Metab. 77 (2002) 260–266.
[36] R.N. Carvalho, T. Solstad, E. Bjørgo, J.F. Barroso, T. Flatmark, Deamidations in recombinant human phenylalanine hydroxylase. Identification of labile asparagine residues and functional characterization of Asn–>Asp mutant forms, J. Biol. Chem. 278 (2003) 15142–15152.
[37] M.A. Digman, C.M. Brown, P. Sengupta, P.W. Wiseman, A.F. Horwitz, E. Gratton, Measuring fast dynamics in solutions and cells with a laser scanning microscope, Biophys. J. 89 (2010) 1317–1327.
[38] R.B. Dalal, M.A. Digman, A.F. Horwitz, V. Vetri, E. Gratton, Determination of particle number and brightness using a laser scanning confocal microscope operating in the analog mode, Microsc. Res. Technol. 71 (2008) 69–81.
[39] T.A. Jones, J.Y. Zou, S.W. Cowan, M. Kjeldgaard, Improved methods for building protein models in electron density maps and the location of errors in these models, Acta Crystallogr.A. 47 (1991) 110–119.
[40] M. Thòròlfsson, B. Ibarra-Molero, P. Fojan, S.B. Peterson, J.M. Sanchez-Ruiz, A. Martinez, L-Phenylalanine binding and domain organization in human phenylalanine hydroxylase: a differential scanning calorimetry study, Biochem. 41 (2002) 7573–7585.
[41] E. Bjørgo, P.M. Knappskog, A. Martinez, R.C. Stevens, T. Flatmark, Partial characterization and three-dimensional-structural localization of eight mutations in exon 7 of the human phenylalanine hydroxylase gene associated with phenylketonuria, Eur. J. Biochem. 257 (1998) 1–10.
[42] A.L. Pey, B. Perez, L.R. Desviat, M.A. Martinez, C. Aguado, H. Erlandsen, A. Gamez, R.C. Stevens, M. Thórólfsson, M. Ugarde, A. Martinez, Mechanisms underlying responsiveness to tetrahydrobiopterin in mild phenylketonuria mutations, Hum. Mutat. 24 (2004) 388–399.
[43] H. Erlandsen, F. Fusetti, A. Martinez, E. Hough, T. Flatmark, R.C. Stevens, Crystal structure of the catalytic domain of human phenylalanine hydroxylase reveals the structural basis for phenylketonuria, Nat. Struct. Biol. 4 (1997) 995–1000.
[44] J.M. Richardson, G.I. Makhatadze, Temperature dependence of thermodynamics of helix-coil transition, J. Mol. Biol. 335 (2004) 1029–1037.
[45] A.J. Stokka, R.N. Carvalho, J.F. Barroso, T. Flatmark, Probing the role of crystallographically defined/predicted hinge-bending regions in the substrate-induced global conformational transition and catalytic activation of human phenylalanine hydroxylase by single-site mutagenesis, J. Biol. Chem. 279 (2004) 26571–26580.
[46] S. Kure, K. Sato, K. Fujii, Y. Aoki, Y. Suzuki, S. Kato, Y. Matsubara, Wild-type phenylalanine hydroxylase activity is enhanced by tetrahydrobiopterin supplementation in vivo: an implication for therapeutic basis of tetrahydrobiopterin-responsive phenylalanine hydroxylase deficiency, Mol. Genet. Metab. 83 (2004) 150–156.
[47] N. Blau, H. Erlandsen, The metabolic and molecular bases of tetrahydrobiopterin-responsive phenylalanine hydroxylase deficiency, Mol. Genet. Metab. 82 (2004) 101–111.
[48] A.C. Muntau, W. Roschinger, M. Habich, H.H. Demmelmair, B. Hoffmann, C.P. Sommhoff, A.A. Roscher, Tetrahydrobiopterin as an alternative treatment for mild phenylketonuria, N. Engl. J. Med. 347 (2002) 2122–2132.

Further reading

[49] V. Novokahtny, K. Ingham, Thermodynamics of maltose binding protein unfolding, Protein Sci. 6 (1997) 141–146.